

RESEARCH

Open Access



# Seismic Behavior of High-Performance Fiber-Reinforced Cement Composites Beam-Column Connection with High Damage Tolerance

Mohammad Hossein Saghafi<sup>1</sup>, Hashem Shariatmadar<sup>1\*</sup> and Ali Kheyroddin<sup>2</sup>

## Abstract

The purpose of this study is to investigate and evaluate the feasibility of using high-performance fiber-reinforced cement composites (HPFRCC) to satisfy the requirement of transverse reinforcement in beam-column joint under seismic loads. The basic mechanical properties of the HPFRCCs are determined by compression, uniaxial tension, and direct shear tests. Four half-scale exterior beam-column connections are cast and tested under cyclic loads. The cracking patterns, hysteresis behavior, ductility, energy dissipation with damping characteristics and joint shear capacity of the HPFRCC beam-column connections are analyzed, investigated, and compared to the cyclic responses of normal concrete connections designed with/without seismic criteria of ACI. The test results revealed that HPFRCC connections considerably enhances shear and flexural capacity and also improved the deformation and damage tolerance behavior in post-cracking stage comparing to normal concrete connections in ultimate stages. Also, the failure mode of HPFRCC specimens changed from shear mode to flexural mode comparing to the connections without seismic details. Severe damages are observed in normal concrete connection designed without considering seismic criteria. Wide diagonal cracking and damage are observed on the designed NC connections under large cyclic displacement at drift 6%. However, in HPFRCC connections, joint remained intact without any cracks and damage until the test end. This implies that the shear stress requirement can be satisfied without any need to the transverse reinforcement in the HPFRCC joint.

**Keywords:** high-performance fiber reinforced cement composites, mechanical properties, strain hardening, beam-column connection, shear performance, hysteresis behavior

## 1 Introduction

Beam-column connections in reinforced concrete structures experience significant shear stresses under lateral displacement induced by earthquakes. This may cause severe connection damage and stiffness reduction in structure. Since 1960s till now, many researchers (Ehsani and Wight 1982; Megget and Park 1971; Durani and Wight 1982; Craig et al. 1984) have conducted

investigations to develop design criteria that assure the proper and adequate behavior of connections in frames under large inelastic deformations. A proper design of beam-column connection in structures needs to satisfy strength and ductility criteria to prevent sudden collapse (Bindhu and Jaya 2010). ACI 318M-11 committee (2011) recommended adequate transverse reinforcement in the joint to prevent shear failure in beam-column joint. A large amount of transverse reinforcement results in steel concentration and make the concrete pouring and compaction difficult. Improper concrete compaction and its reduced quality, in turn, cause lower deformation capacity and connection vulnerability during earthquakes (Henager 1977). Observations from the

\*Correspondence: shariatmadar@um.ac.ir

<sup>1</sup> Department of Civil Engineering, Ferdowsi University of Mashhad, P.O. Box 91775-1111, Mashhad, Iran

Full list of author information is available at the end of the article  
Journal information: ISSN 1976-0485 / eISSN 2234-1315

previous earthquakes confirm that brittle failure mechanisms result in severe damage or even collapse of structures. Beam-column connection failure due to shear failure or reinforcement sliding is frequent in these mechanisms and have been observed in 2009 L'Aquila earthquake, Italy (Fig. 1) (Metelli et al. 2015).

Over the past 25 years, numerous studies (Craig et al. 1984; Henager 1977; Gefken and Ramey 1989; Jiuru et al. 1992; Filiatrault et al. 1995; Bayasi and Gebman 2002) have been done for investigation and evaluation of the effects of fiber reinforced concrete (FRC) in order to reduce the reinforcement concentration and improve seismic performance in beam-column joints. Recently, FRC materials used in research studies on beam-column joints generally include normal concrete with steel fibers. In spite of achieving a highly desirable tensile response compared to conventional concrete, these fiber cement composites show a softening tensile response after the first cracking, while in the high-performance fiber reinforced cementitious composites (HPFRCCs), strain hardening behavior is observed by the formation of additional cracks (Fig. 2). The results of previous studies indicate that FRC with 1.2% to 2% volumetric steel fibers can be used as an alternative to part of confining reinforcement

in column-beam joints. Also, the conditions for anchorage in the longitudinal reinforcement of the beam and column in the joints have been improved with the use of steel fiber reinforced concrete (Jiuru et al. 1992). Since these materials exhibit softening tensile response after the formation of the first cracks, despite the prevention of premature damage, this will limit the ability to withstand large tensile stresses, making the FRC improper choice to replace the transverse reinforcement in beam column joints with high stress. The higher strain capacity of HPFRCCs is idealized to be used in the plastic hinge of beam-column joints to eliminate the need for transverse reinforcement details (Parra-Montesinos et al. 2005; Hossein Saghafi and Shariatmadar 2018). Also, the necessity of special transverse reinforcement with high energy dissipation and lower stiffness properties has been resolved (Saghafi et al. 2016; Kim et al. 2008).

Parra-Montesinos et al. (2005) tested two full-scale beam-column connections where the HPFRCC was used in joint and in plastic hinges of the beam. In these specimens, shear reinforcement were eliminated in the joint area and distance of stirrups in plastic hinge area of the beam was increased. Test results showed that these connections were able to perform properly under large shear loads. Moreover, the observations showed that joint reinforcement can be omitted and still achieve the required shear strength (Parra-Montesinos et al. 2005).

Hemmati et al. (2013) investigated the effects of using HPFRCC material in concrete beams and frames. The results of the tests showed that load carrying capacity and deformation capacity of beams and frames were increased using HPFRCC. In addition, plastic hinge length as well as its rotation capacity were higher in HPFRCC compared to those in normal concrete specimens (Hemmati et al. 2013, 2016).

Yuan et al. (2013) investigated the behavior of exterior beam-column connections fabricated by engineered

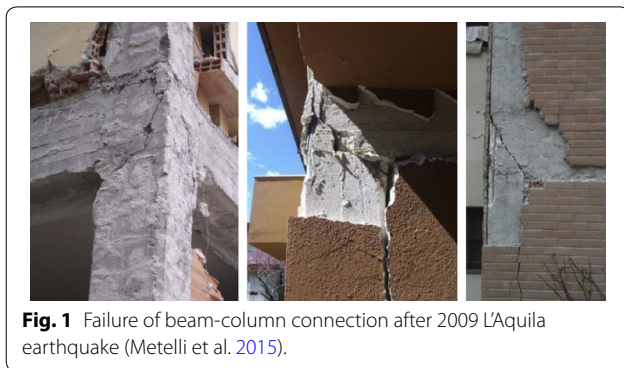


**Fig. 1** Failure of beam-column connection after 2009 L'Aquila earthquake (Metelli et al. 2015).

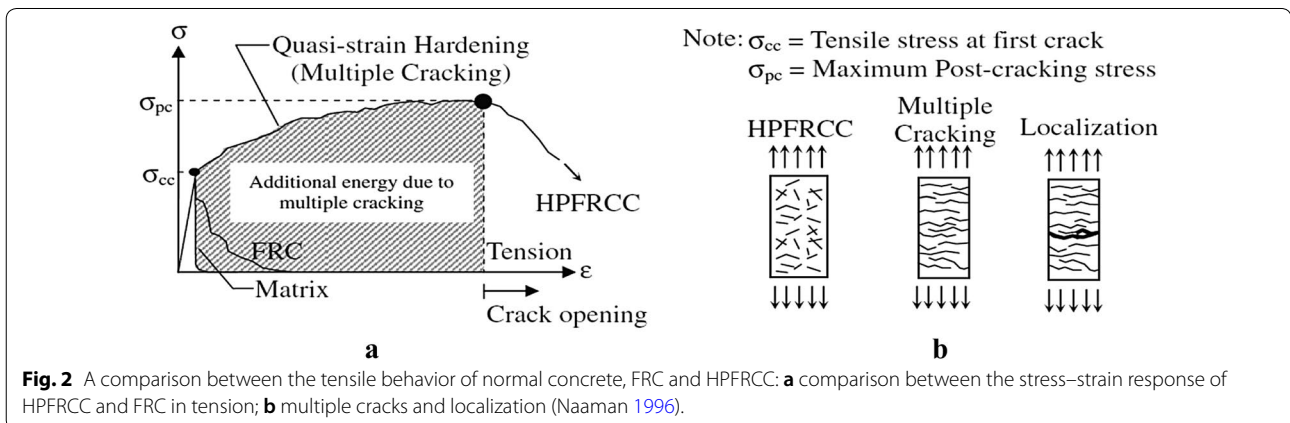


**Fig. 2** A comparison between the tensile behavior of normal concrete, FRC and HPFRCC: **a** comparison between the stress–strain response of HPFRCC and FRC in tension; **b** multiple cracks and localization (Naaman 1996).

cementitious composites (ECC) under cyclic load. The results have shown that the use of ECC instead of normal concrete resulted in higher shear strength and damping property (Yuan et al. 2013).

Zhang et al. (2015) used PolyPropylene Engineered Cementitious Composites (PP-ECC) in exterior beam-column railway bridges with rigid frames to prevent reinforcement concentration and to reduce a large amount of transverse reinforcement. The results show that substitution of transverse reinforcement by PP-ECC in beam-column connections of railway bridges with rigid frames has a positive effect on its behavior (Zhang et al. 2015).

Chidambaram and Agarwal (2015) investigated the behavior of exterior beam-column connections fabricated by different cementitious composites using a combination of steel and polypropylene fibers under cyclic load. The results have shown that the use of HPRCC material instead of normal concrete resulted in higher stiffness, higher load carrying capacity and energy dissipation (Chidambaram and Agarwal 2015).

Said and Razak (2016) investigated the effect of using ECC in exterior beam-column reinforced concrete connection under cyclic loading. ECC connection caused a significant increase in shear and bending capacity and improved the deformation behavior and failure toughness compared to the normal concrete specimen in ultimate states and failure (Said and Razak 2016).

Especially, few experimental investigations has been carried out to study the effect of HPRCC composites on the behavior of beam-column connections under cyclic load. Most of the available studies about HPRCC have focused on interior beam-column connections. Moreover, HPRCC used in the previous studies are fabricated using polypropylene, polyethylene and polyvinyl alcohol by 2–3% in volume ratio. Besides, scarce experimental studies are implemented to consider the shear behavior of HPRCC connections. In the present study, the possibility to achieve high displacement and damage tolerance capacity in frames designed with/without seismic details for connections using HPRCC materials has been evaluated. Reducing the required transverse reinforcement, as well as reducing the workforce, and more importantly, achieving highly damage tolerant structures reduces the need for post-earthquake structural repairs. Two types of cementitious composites including steel fiber alone

and hybrid fibers (steel and macro-synthetic fibers) with strain hardening behavior are used. In the first part of the experimental tests, strain hardening properties of HPRCC is determined using uniaxial tension test and direct shear test to provide a better understanding. In the second part of the tests, to show the benefit of (a) using the transverse reinforcement for concrete confinement (b) replacing the normal concrete with HPRCC and comparison with the normal concrete with/without the transverse reinforcement to satisfy the need for confining reinforcement (transverse) and the related construction problems in beam-column joint, four exterior beam-column connections by the scale of  $\frac{1}{2}$  are fabricated and tested under cyclic load.

## 2 Preparation of HPRCC Mixtures

Different mixture ratios are considered to achieve acceptable strain hardening behavior for HPRCC (Saghafi et al. 2017), and according to Table 1, the best mix design of mortar in specimen with weight mix ratio has been adopted. The sand in mix design include crushed particles with a grain size of 0.1 mm to 4.75 mm and 1 mm in average.

Firstly, water, cement, and sand are mixed for 5 min to prepare HPRCC specimens. After hydration of cement, almost half of the superplasticizer is added to the mixture and mixed for another 5 min. At the next stage, silica fume and the remained superplasticizer is added to the mixture to achieve proper workability. Finally, the fibers are gradually added to the mortar. Since the mix design is constant, the only difference between HPRCC specimens is the type of applied fibers. Two types of fibers are used: (1) hooked steel fiber and (2) macro synthetic fiber (Fig. 3). It should be noted that the macro synthetic fiber are obtained by mixing polypropylene, polyethylene woven and modified copolymer individuals. These fibers are shown in Fig. 4. Fiber properties are presented in Table 2 and two types of HPRCC as described in Table 3 are used in this study.

## 3 The Experimental Program

### 3.1 Mechanical Properties

The cylinder specimens with 100 mm diameter and height of 200 mm have been tested under uniaxial compression test in accordance with ASTM C39/C39M-10

**Table 1** Mix design for HPRCC mortar and normal concrete.

| TYPE                  | Admixture (superplasticizer)     | Cement | Silica fume | Water | Sand | Gravel |
|-----------------------|----------------------------------|--------|-------------|-------|------|--------|
| HPRCC mortar ratio    | 0.14% binder <sup>a</sup> weight | 1      | 0.1         | 0.28  | 1    | –      |
| Conventional concrete | –                                | 1      | –           | 0.45  | 1.72 | 1.72   |

<sup>a</sup> Binder = cement + silica fume.

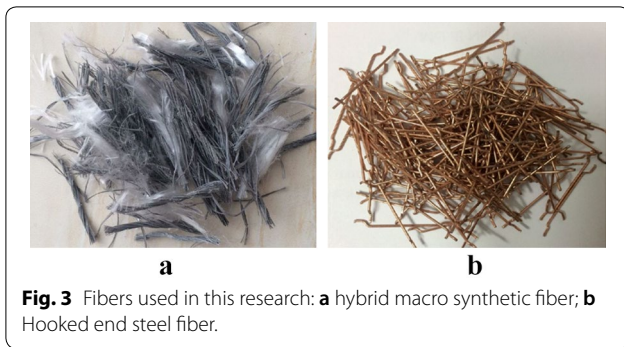


**Fig. 3** Fibers used in this research: **a** hybrid macro synthetic fiber; **b** Hooked end steel fiber.

standard (2010). The uniaxial tension tests have been tested on I-shape specimens in accordance with recommendations of Japan Society of Civil Engineers (JSCE) (2008). Using electronic universal testing machine under displacement controlled condition having loading velocity of 0.1 mm/min and designed test setup (Fig. 5), the specimens positioned on the test system. The load values and length changes have been measured during the tests. A linear variable differential transformers (LVDT) has been installed at center of the tensile specimen and along the loading path to determine the length changes.

The Z-shape compression specimens are preferred due to convenience in loading and data analysis to evaluate the mechanical properties of HPCFRCCs under shear loads. Though, large tensile stresses are available at the end of crack propagation area which show increments of cracks in tests are not only under pure

**Table 3** The type of used concrete.

| Specimen ID | Volume of fiber        |                         |
|-------------|------------------------|-------------------------|
|             | Hooked end steel fiber | Macro (synthetic fiber) |
| NC          | –                      | –                       |
| HPFRCC-A    | 1%                     | 1%                      |
| HPFRCC-B    | 2%                     | –                       |

shear modes but in a hybrid mode which includes shear modes and crack widening. JSCE has proposed a method to define the shear strength of FRC using direct shear test. The initiated stresses in this test are only due to pure shear loads and no hybrid mode is observed. Mirsayah et al. found that sometimes based on JSCE proposed method, the cracks are often deviated. Therefore, a surface split is proposed to predict the failure plane (Mirsayah and Banthia 2002). Shear test is conducted on 250 × 75 × 75 mm prismatic specimens (JSCE, G 553-1999, 2005). To assure that the fracture will occur in predefined locations, section reduction and gap creation around the specimens is done when the specimens are in the molds. Using electronic universal testing machine under displacement controlled condition having loading velocity of 0.1 mm/min and designed test setup (Fig. 6), the specimens positioned on the test system. Displacement of middle area in the

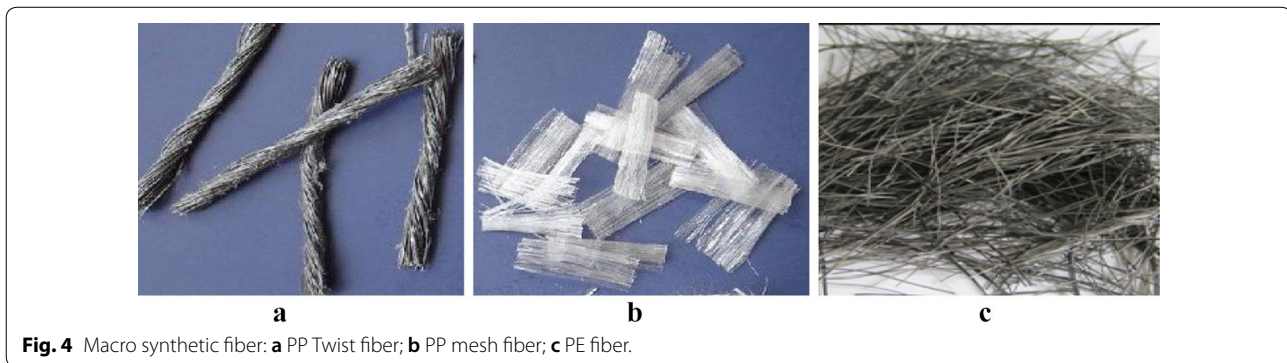


**Fig. 4** Macro synthetic fiber: **a** PP Twist fiber; **b** PP mesh fiber; **c** PE fiber.

**Table 2** Main properties of fiber used in this study.

| Name                   | Type of fiber                        | Length (mm) | Diameter (mm) | Aspect ratio | E (Gpa) | Tensile strength (Mpa) | Density (kg/cm <sup>3</sup> ) × 10 <sup>-3</sup> |
|------------------------|--------------------------------------|-------------|---------------|--------------|---------|------------------------|--|
| Hooked end steel fiber | Steel fiber                          | 35          | 0.80          | 43.75        | 212.00  | 1100                   | 7.85   |
| Macro synthetic fiber  | Polypropylene (Twist and mesh Fiber) | 54          | 0.09          | 600.00       | 6.90    | 450–800                | 0.91   |
|                        | polyethylene                         | 48          | 0.31          | 154.83       | 4.70    | 550–660                | 0.91   |

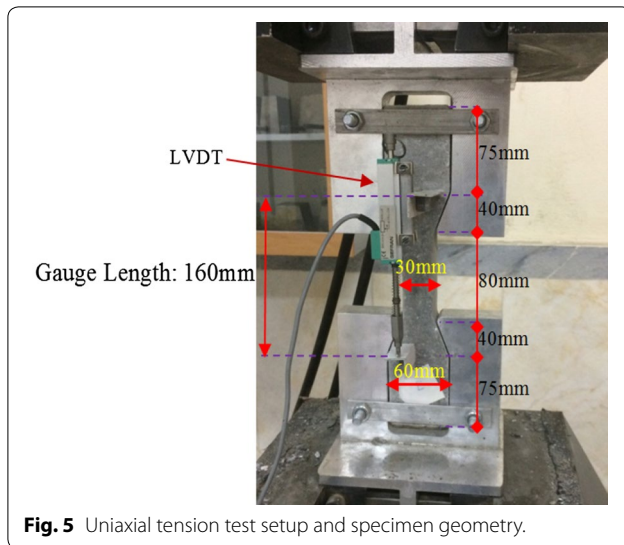


**Fig. 5** Uniaxial tension test setup and specimen geometry.

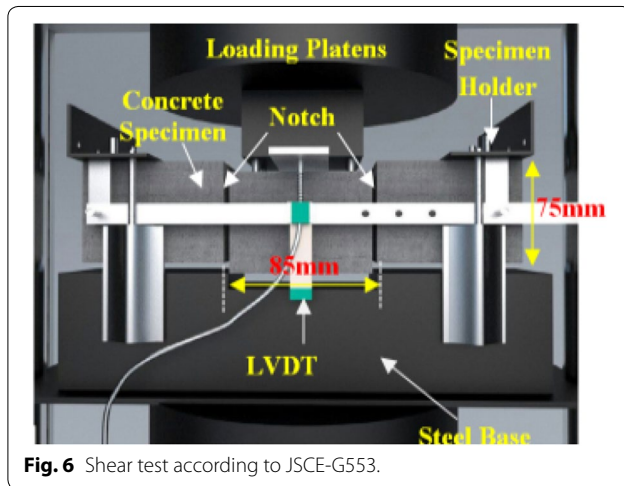


**Fig. 6** Shear test according to JSCE-G553.

lower face of prism is measured using a LVDT. The mechanical test program is given in Table 4.

### 3.2 Beam-Column Joints

Four half-scale exterior beam-column connections with the same sizes have been fabricated in structural lab of Ferdowsi Mashhad University and tested under

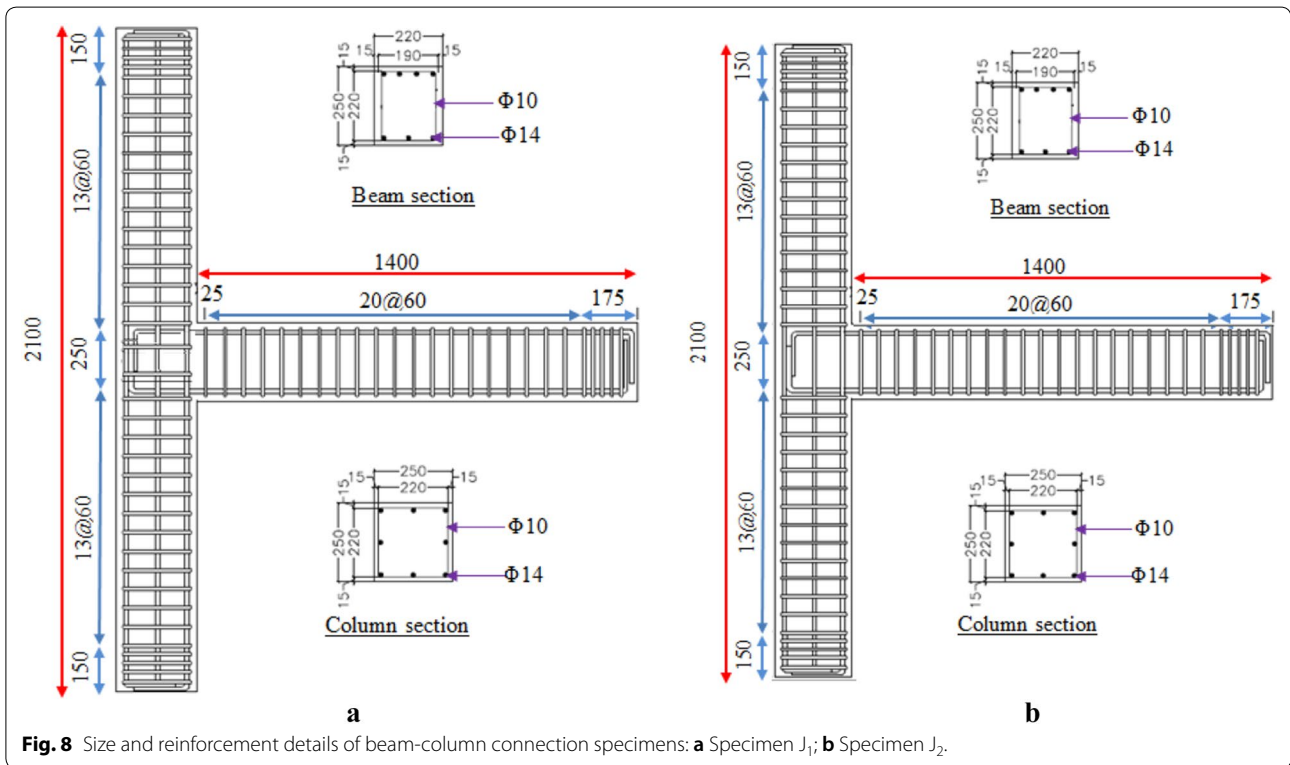
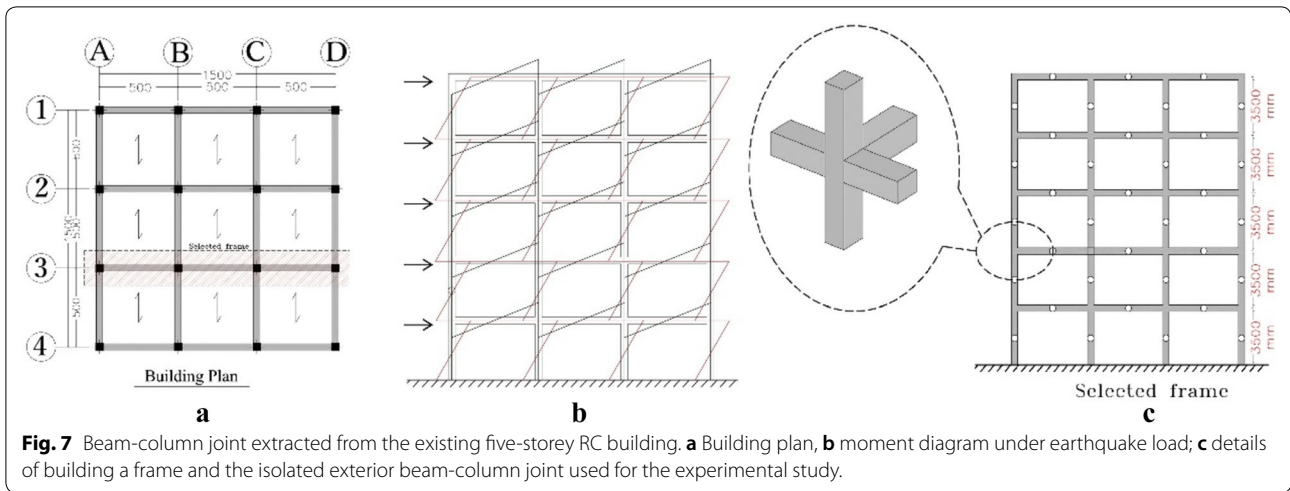
quasi-static increasing cyclic load. The exterior beam-column connections are related to a 5-story existing structure with story height of 3.5 m and an effective span length of 5 m which is investigated after separation. In the design of beam-column connections, it is assumed that flexural inflection point is located at the mid-height of column and beam as shown in Fig. 7. To design the specimen, the ratio between bending strengths of the column to the beam is calculated and the strong column-weak beam concept is considered. The sizes of longitudinal reinforcement in beams and columns are the same for all specimens. The affecting parameters in the test are: (a) stirrup details in joint, (b) type of concrete. Two different details of transverse reinforcement are included with seismic reinforcement detailing and without seismic reinforcement detailing (named as  $J_1$  and  $J_2$  respectively).  $J_1$  stirrup details for beam-column connection is designed according to the requirements of ACI Committee 318M-11 code (2011) in a way that the longitudinal and transverse reinforcement for beam and column and connection satisfy the seismic requirements of the code and provide adequate shear strength in joint according to code criteria. Specimen  $J_2$  for non-seismic beam-column connection with inadequate shear strength at the joint due to non-stirrup inclusion in the joint zone.

Except for the transverse reinforcement in joint, longitudinal and transverse reinforcement in beams and columns satisfy the seismic requirements of ACI 318M-11 code (2011). The two reinforcement details are shown in Figs. 8 and 9. To investigate the effect of using HPRCC material instead of transverse reinforcement in joint, two different concrete pouring patterns using normal concrete and HPRCC are considered as it is shown in Figs. 10 and 11. In the first pattern (called NC) all beam-column connection is fabricated using normal concrete. In the second pattern (HPRCC), HPRCC material is used in the joint as well as for a length equal to two times as beam depth in beam and two times as column depth in the column (Said and Razak 2016; Qudah and Maalej 2014). Normal concrete is used in the other regions. Full details of beam-column connections with the mentioned concrete pouring patterns are presented in Table 5. The properties of applied reinforcement are tabulated in Table 6.

**Table 4** Mechanical test program.

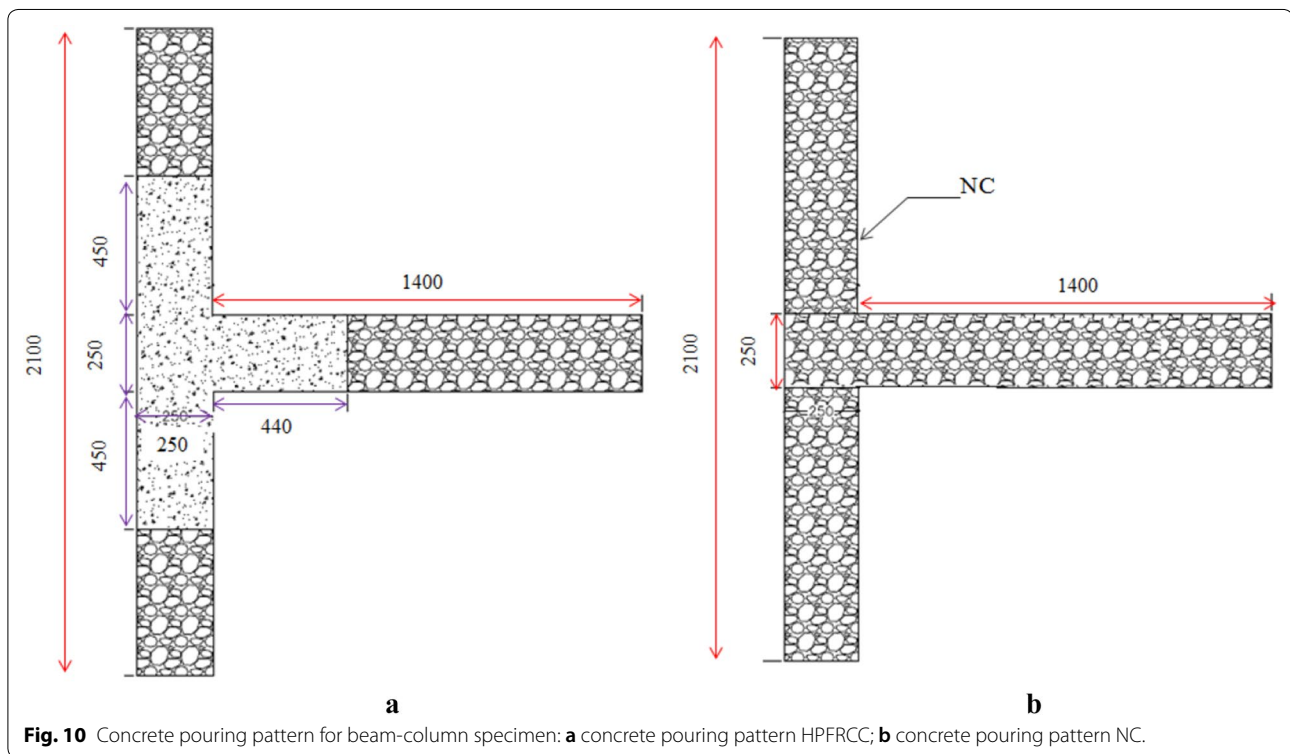
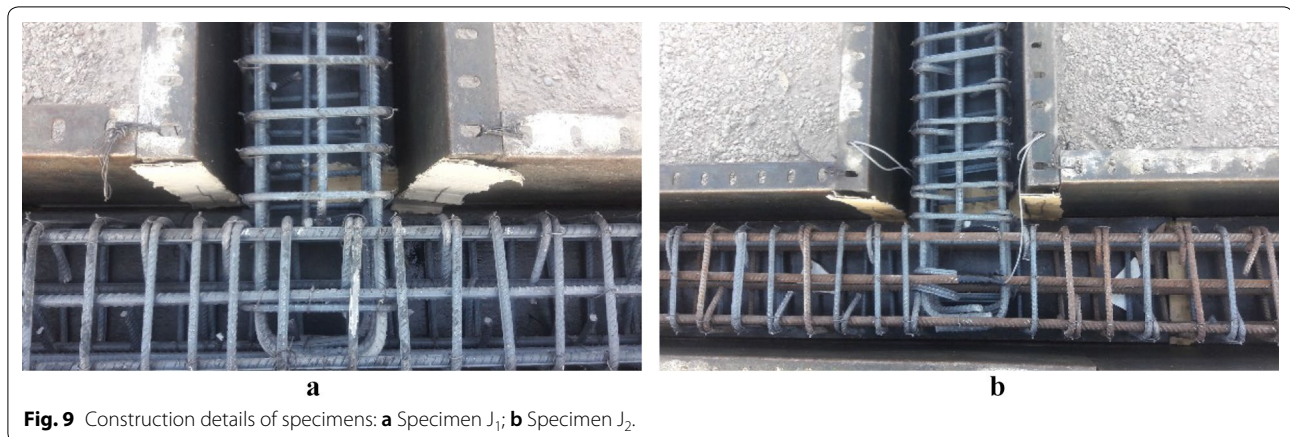
| Test                | Compression test       | Tension test         | Shear test             |
|---------------------|------------------------|----------------------|------------------------|
| Specimen size       | 100 × 200              | 30 × 30 × 330        | 75 × 75 × 250          |
| Procedure adopted   | ASTMC39/C39M-10 (2010) | JSCE-N82-2008 (2008) | JSCE-G-553-1999 (2005) |
| Number of specimens | 4 per mix              | 4 per mix            | 3 per mix              |

Unite: mm.



A schematic view of test arrangement, support condition and loading is shown in Fig. 12. Support points are in fact the moment curve turning points under a lateral load of the real frame. It should be noted that beam and column in the test are rotated 90 degrees and the load is applied to beam, as it can be seen in Fig. 12, along the direction perpendicular to the ground surface. The column ends are pinned and only the rotation is permitted. For all specimens, constant axial load of 200 kN equal

to  $0.15 f'_c A_g$  is applied to a column by hydraulic jack of 300 kN capacity using load control method. When 200 kN constant axial load is applied, a hydraulic jack of 600 kN capacity is used to induce lateral cyclic displacement on beam end. The applied load on the specimen is measured by an S-shape load cell (Fig. 13) which is capable of recording in dual direction and data are transferred to a computer system. The distance between load point and column face is 1250 mm. Lateral displacement of



beam end is measured and recorded by an LVDT, with a displacement capacity of 150 mm. Drift parameter is calculated by dividing lateral displacement at load application point to the distance of the point from column face. Lateral load applied on the beam using displacement control with three cycles in each drift angle. This cyclic loading history is continued by drifts (0.5% to 6% by increasing step of 0.5%). The cyclic load protocol is shown in Fig. 14. To measure the strain of reinforcement bar in different loading stages, five strain gauges are installed on longitudinal and transverse reinforcement

for each connection specimen. According to Fig. 15, five LVDTs are used to measure the rotation of the beam and distortion of the joint.

## 4 Results and Discussion

### 4.1 Mechanical Properties of HPFRCC

Uniaxial compressive and tensile stress–strain relationship for normal concrete and HPFRCC specimens are shown in (Fig. 16a, b) and specimen results obtained by direct shear test is shown in Fig. 16c as sliding



Fig. 11 Concreting pattern of HPFRCC.

Table 5 Details of exterior beam-column connection.

| ID    | Concrete in joint | Reinforcement pattern | Joint transverse reinforcement | Beam reinforcement (%)   | Beam and column transverse reinforcement    | Column reinforcement (%)                               |
|-------|-------------------|-----------------------|--------------------------------|--|---|--|
| C1    | NC                | J1                    | Ø10@60 mm                      | All specimens are reinforced with 4Φ14 at top and 3Φ14 at bottom (ratio = 1.95%) | All specimens are reinforced with Φ10@60 mm | All specimens are reinforced with 8Φ14 (ratio = 1.97%) |
| C2    | NC                | J2                    | 0                              |  |   |  |
| SC2-A | HPFRCC-A          | J2                    | 0                              |  |   |  |
| SC2-B | HPFRCC-B          | J2                    | 0                              |  |   |  |

Table 6 Properties of applied reinforcement.

| Diameter of rebar | Yield strength (MPa) | Ultimate strength (MPa) | Yield strain (%) | Ultimate strain (%) |
|-------------------|----------------------|-------------------------|------------------|---------------------|
| 10                | 380                  | 440                     | 0.19             | 17                  |
| 14                | 430                  | 673                     | 0.2              | 16                  |

(displacement)-shear stress curve. The results are summarized in Table 7.

The test results indicate that the compressive strength and corresponding strain in HPFRCC specimens are clearly higher than those of the normal concrete specimens. The strength of cylindrical HPFRCC-A and HPFRCC-B specimens are about 1.29 and 1.58 times, greater than those of normal concrete, respectively. The tension tests revealed that HPFRCC specimens show strain hardening behavior accompanied with multiple cracks. The average tensile strength for each of HPFRCC-A and HPFRCC-B specimens is about 2.15 and 2.31 times greater than that of the normal concrete specimens, respectively. Moreover, the average ultimate strain at ultimate tensile strength in each of HPFRCC-A and HPFRCC-B specimens is about 40.72 and 42.22 times greater than that of the normal concrete specimens, respectively. The average shear strength of HPFRCC-A and HPFRCC-B specimens are about 4.2 and 4.82 times

greater than that of the normal concrete specimens, respectively.

#### 4.2 Beam Column Joints

To investigate the effect of using high strain material on seismic behavior of specimens and the feasibility of reducing transverse reinforcement in joint, behavior under cyclic loads of the tested beam-column connections is evaluated based on hysteresis behavior, envelope load-deformation curve, energy dissipation, stiffness and strength reduction and damage characteristics. Details of the parameters used for evaluation and interpretation of test results are as follows.

##### 4.2.1 Failure Mode and Crack Propagation

Damage pattern on C1 specimen is shown in Fig. 17a. The first bending cracks are observed at the bottom of the beam at a distance of  $d/2$  from the column face at a drift of 0.5%. Longitudinal reinforcement yield at the drift of 1%. Concrete cover spalling over the reinforcement in joint and diagonal cracks in joint area are initiated in drift of 2%. Most of the flexural micro cracks in beam concentrate near column face result in formation of the plastic hinge in the beam. By increasing the applied load, crack extension and opening is observed in the joint and for the cycles with drift larger than 3.5%, the opening of shear cracks in the joint is measured to be up to 10 mm.

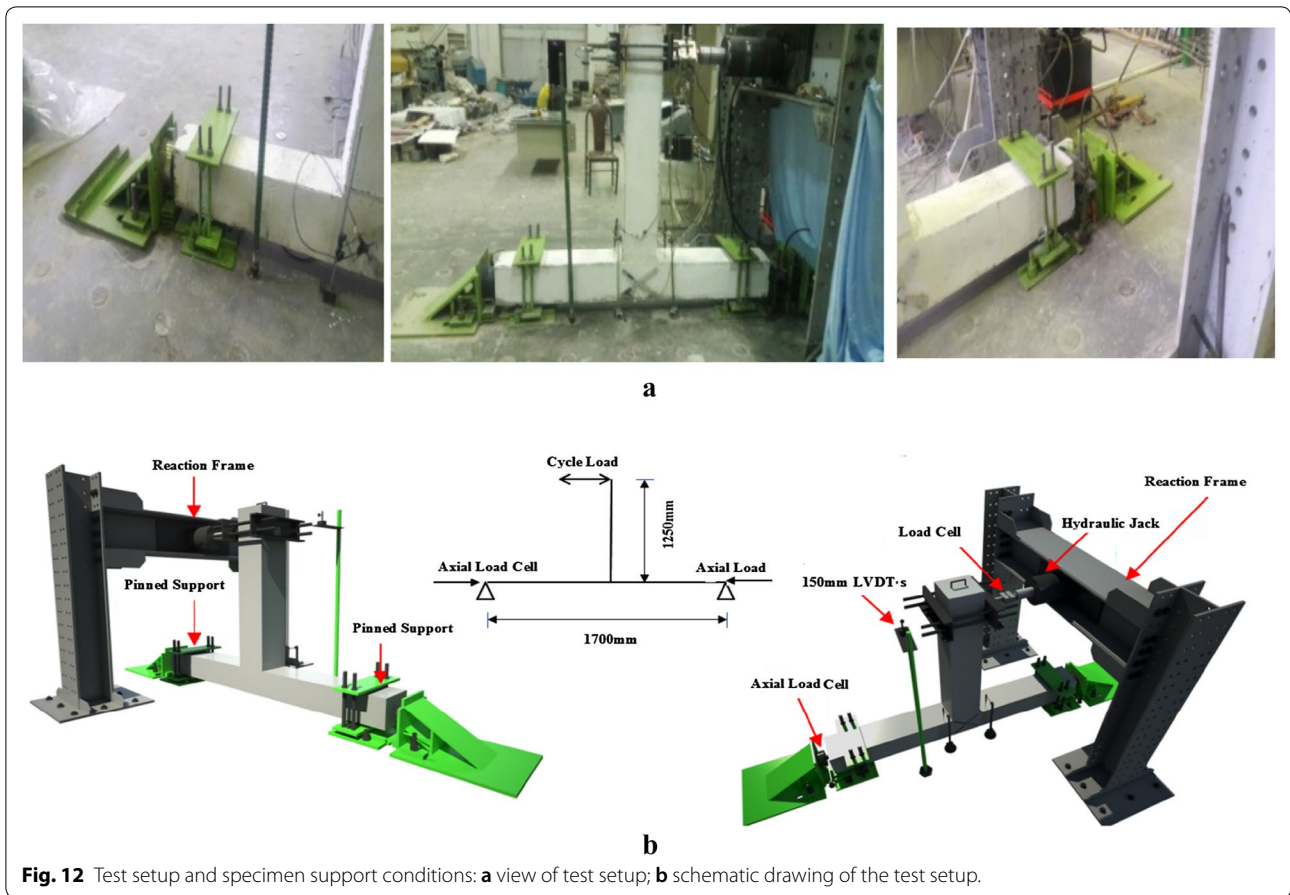


**Fig. 12** Test setup and specimen support conditions: **a** view of test setup; **b** schematic drawing of the test setup.

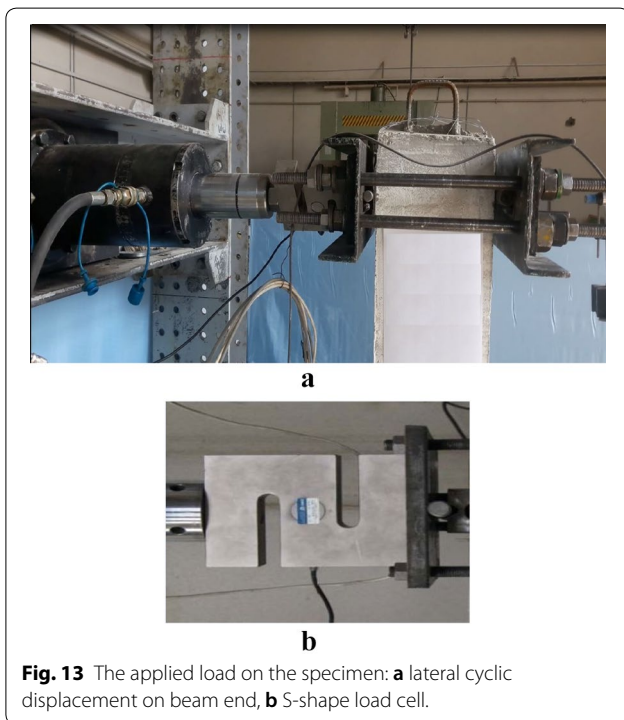


**Fig. 13** The applied load on the specimen: **a** lateral cyclic displacement on beam end, **b** S-shape load cell.

Furthermore, damage is mainly concentrated in the beam end and cracks can be easily observed due to their opening and closing under increasing cyclic load. The width of the formed cracks in beam after the distance of  $d/2$  from column face are very small and their participation in energy dissipation at the next load steps is not considered. Since it seems that most of the energy dissipation is done in damaged area at beam end and near the column face, many of the cracks are formed before achieving the ultimate load, while few cracks are formed after the application of the peak load.

In C2 specimen, the first cracks are formed similarly to those in C1 specimen. However, diagonal cracks in joint are initiated in the drift of 1% which show the connection failure is imminent. The number and size of flexural and diagonal cracks go up by load drift increase. Longitudinal reinforcement yield in the drift of 1%. From the drift of 1.5%, no new crack is formed in beam and only the opening of beam end cracks near column face is observable. In drift of 2%, an increase in crack width is observed at beam end region and crack propagation in the joint is seen in the form of concentrated diagonal cracks. From drift of 3%, loading capacity is deteriorated and cracks in

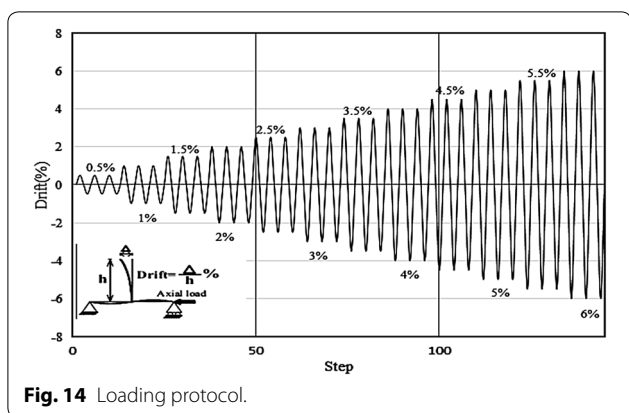


**Fig. 14** Loading protocol.

joint are widening. In drift of 4.5%, concrete in the joint is laminating and failed and the longitudinal reinforcement appeared. Although joint is severely damaged, lateral cycles are continued until drift of 6%. The absence of column stirrups in connection area resulted in the shear failure of the connection. This phenomenon is clearly shown in failure pattern of C2 specimen in Fig. 17b. Moreover, due to the incomplete opening of flexural micro cracks of beam outside of joint at loading initiation and the next loading steps, and also due to the concentration of damage in the joint area, energy dissipation of flexural cracks is not considered.

As it can be seen from Fig. 17c, d, regular propagation of cracking has been observed in specimens with HPRC material. The first cracking in beam end at a distance of  $d/4$  from column face occurred in the drift of 0.5%.

All the cracks observed in the beam are formed within a distance, about 800 mm from the face of the column. The distance between the cracks varies between 43 and 180 mm and the crack lengths are between 55 and

190 mm. The width of formed micro cracks in the beam is not noticeable. In drift of 2%, minor damages in the form of many flexural micro cracks and yield of some beam longitudinal reinforcement in connection area and beam end region are observed. The initiation of micro diagonal cracks in HPRC specimens is observed in the drift of 2%. Averagely from the drift of 3%, opening of cracks, load carrying capacity deterioration and local damages in HPRC material in beam plastic hinge area and formation of no new crack in joint resulted in the formation of the flexural plastic hinge in the beam. Due to opening and closing of the localization of cracks in beam end under increasing cyclic load, crack width reaches to 12 mm at the drift of 6%. By increase of the applied drift, opening and closing of shear cracks without a crack propagation in the joint area was observed accompanied by the formation of small micro cracks. The maximum opening of shear cracks in joint in these specimens is measured as 0.5 mm at the drift of 6%. Moreover, adequate shear strength in connections without the occurrence of local shear cracks is provided and this allows for the formation of plastic hinges in beam and local damages of HPRC material in the plastic hinge area. Yielding of longitudinal reinforcement of the beam in these specimens begins in higher load and drifts compared to that in normal concrete specimens. This can be attributed to higher adhesion strength, higher conjunction, better consistency between steel reinforcement and HPRC and higher displacement capacity before failure in HPRC.

**4.2.2 Cyclic Load–Drift Response**

Load–drift hysteresis response during loading cycles is the most important factor for evaluation of seismic behavior of structure components. The hysteretic

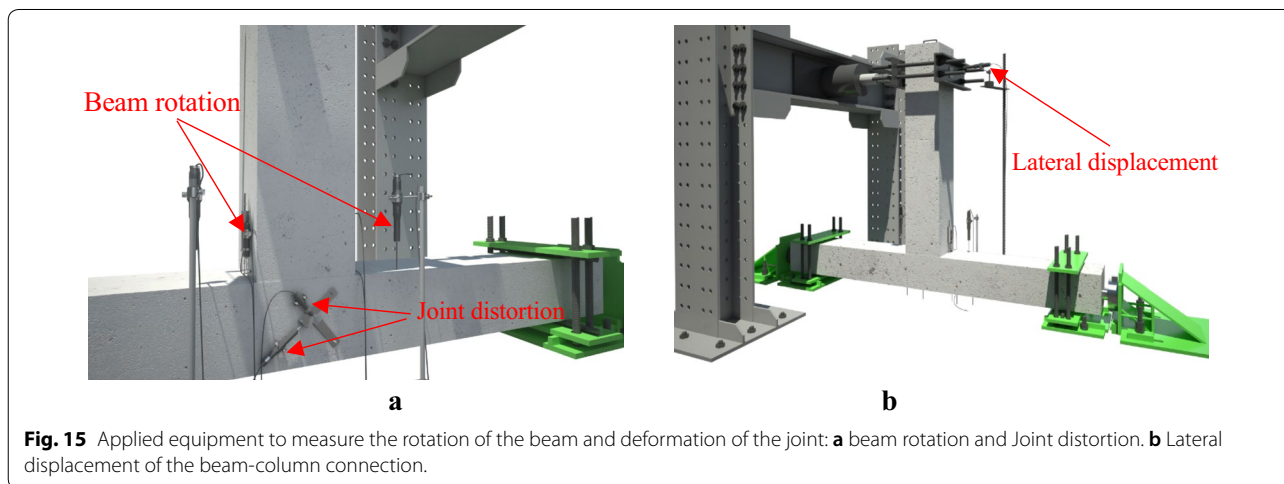


**Fig. 15** Applied equipment to measure the rotation of the beam and deformation of the joint: **a** beam rotation and Joint distortion. **b** Lateral displacement of the beam-column connection.

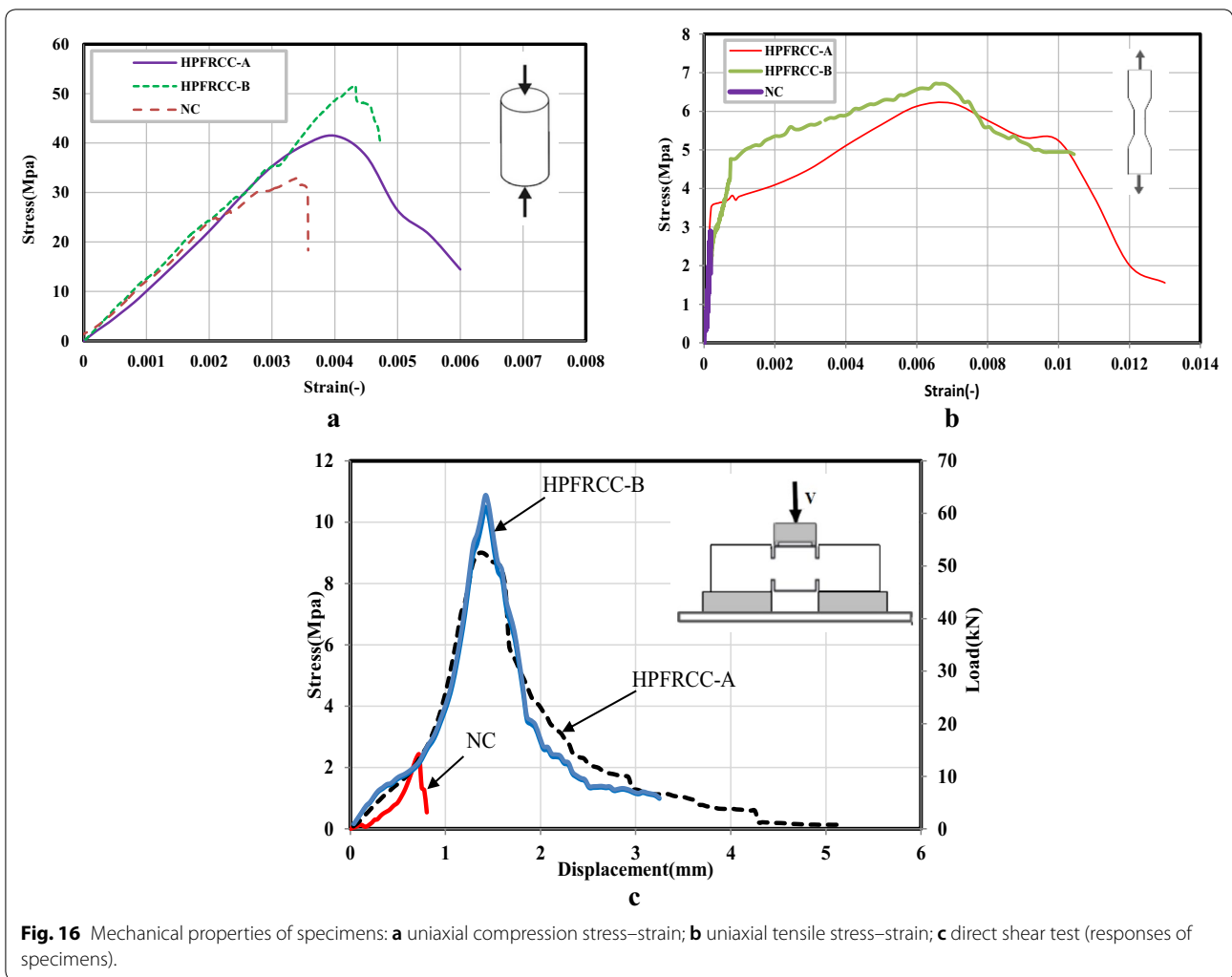


**Table 7** Test results for mechanical properties.

| Specimen | Cylindrical compression test |   | Uniaxial tension test  |   | Direct shear test    |
|----------|------------------------------|---|------------------------|---|----------------------|
|          | Compression strength (MPa)   | Ultimate compressive strain (after peak load) (%) | Tensile strength (MPa) | Ultimate tensile strain (corresponding to the tensile strength) (%) | Shear strength (MPa) |
| HPFRCC-A | 41.47                        | 0.60  | 6.2                    | 0.733   | 8.98                 |
| HPFRCC-B | 50.57                        | 0.47  | 6.7                    | 0.760   | 10.31                |
| NC       | 31.87                        | 0.35  | 2.9                    | 0.018   | 2.14                 |

behavior and the envelope curves for peak displacement points at first reversal of cycles (Elwood et al. 2007) in the specimens are shown in Fig. 18 and the results are presented in Table 8. Normal concrete specimen with seismic details (C1) shows ductile response without pinching or significant strength loss until the test end. This desirable behavior confirms the adequacy of

shear reinforcement and development length of beam longitudinal reinforcement in connection area when satisfying the requirements of ACI 318M-11 (2011) for beam-column connection of reinforced concrete structure. Normal concrete specimen that is designed ignoring the seismic details (C2) shows significant pinching

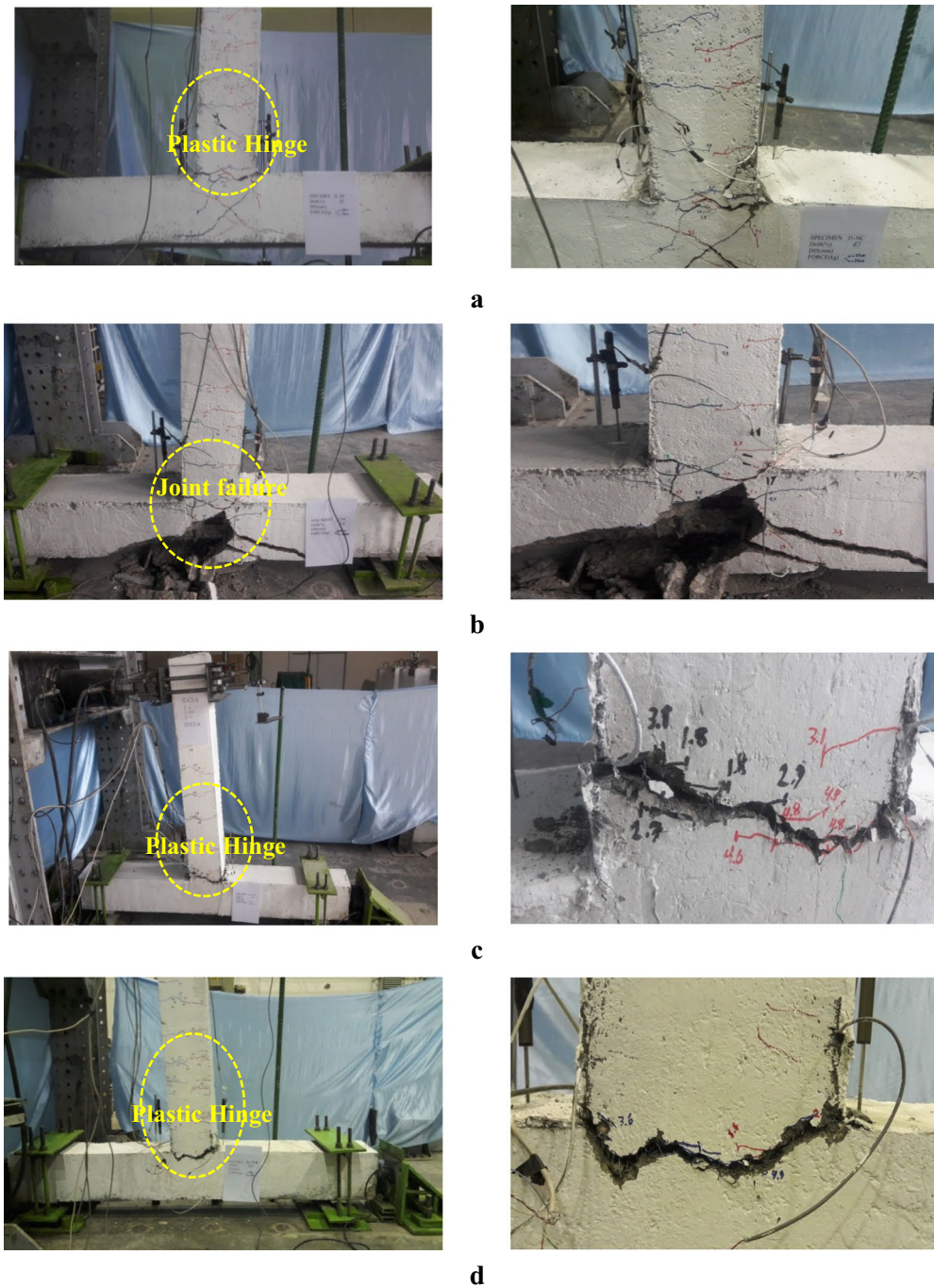


**Fig. 17** Cracking pattern and failure mode in drift of 6%: **a** C1 specimen; **b** C2 specimen; **c** SC2-A specimen; **d** SC2-B specimen.

and continuous stiffness and strength deterioration by displacement increasing compared to that of C1 specimen. Formation of shear cracks in initial loading steps in C2 specimen results in premature sliding of beam longitudinal reinforcement and concrete crushing in connection area. This in turn results in shear failure.

Details of transverse reinforcement and confinement condition in joint of C1 specimen prevents the premature beam longitudinal reinforcement sliding and shear failure, compared to C2 specimen. Furthermore, load carrying capacity deterioration rate after the peak load application is decreased.

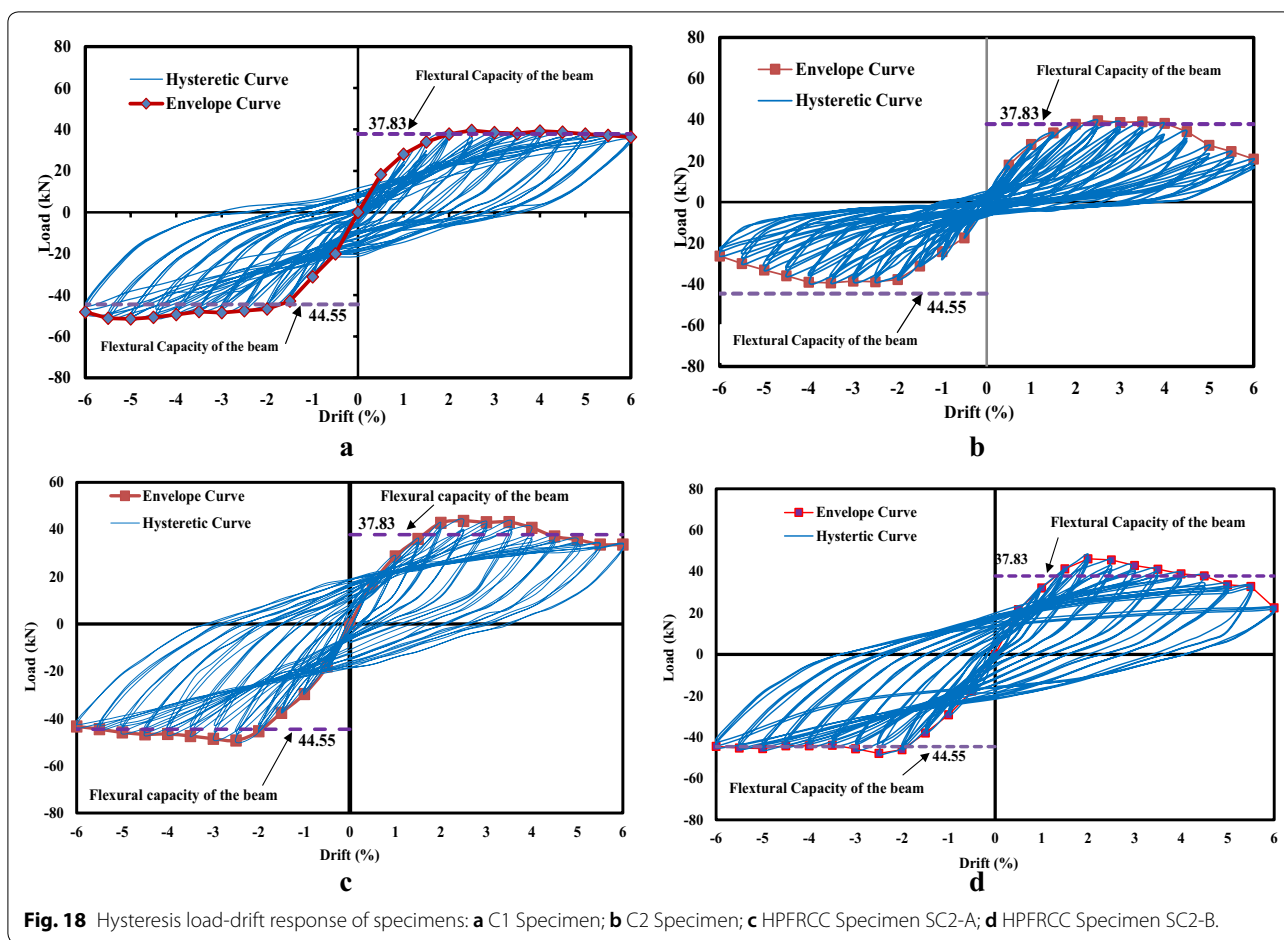


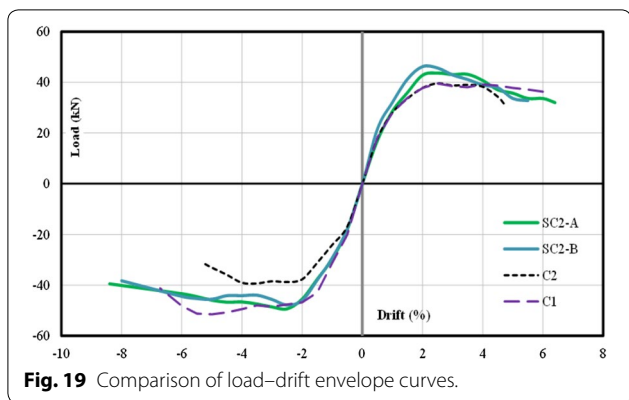
Fig. 18 Hysteresis load-drift response of specimens: a C1 Specimen; b C2 Specimen; c HPFRCC Specimen SC2-A; d HPFRCC Specimen SC2-B.

Table 8 Peak load and ductility factor in negative and positive directions.

| Specimen | Peak load (kN) |          | Average peak load (kN) | Displacement at yield point (mm) |          | Displacement at 20% drop of peak load (mm) |          | Ductility factor |          |
|----------|----------------|----------|------------------------|----------------------------------|----------|--|----------|------------------|----------|
|          | Push (+)       | Pull (-) |                        | Push (+)                         | Pull (-) | Push (+)                                   | Pull (-) | Push (+)         | Pull (-) |
| C1       | 39.18          | 51.58    | 45.34                  | 16.59                            | 20.45    | 75   | 84       | 4.52             | 4.1      |
| C2       | 38.59          | 38.74    | 38.66                  | 15.75                            | 18.94    | 58.68                                      | 66.64    | 3.72             | 3.51     |
| SC2-A    | 43.65          | 47.82    | 46.49                  | 18.2                             | 22.33    | 80   | 105      | 4.39             | 4.7      |
| SC2-B    | 46.2           | 47.82    | 47.02                  | 16.96                            | 21.2     | 68.75                                      | 100      | 4.05             | 4.7      |

The response of beam-column connection confirms that the use of HPFRCC results in improvement of load carrying capacity and increase the area under the hysteresis loops, compared to those of normal concrete specimens C1 and C2. Consequently, the proposed method is proper to be used in high seismic area. Stable behavior continues in HPFRCC specimens respectively until drift of 5.5% and 6%. In HPFRCC specimens, for lateral drift higher than 2%, inelastic rotations in beam area near column face is mainly governing and the

behavior of the other connection parts are in cracked elastic range. After the application of peak load, and due to the opening of cracks at beam end and damage of HPFRCC material in beam, inelastic behavior of plastic hinge results in slight strength reduction of connection. In SC2-B specimens at drift angle of 6%, load carrying capacity is dramatically reduced due to the failure of top longitudinal reinforcement in beam, which shows better behavior of HPFRCC-A specimen in large drifts. When the load direction is reversed,



only the bottom longitudinal reinforcement in beam participate in load carrying.

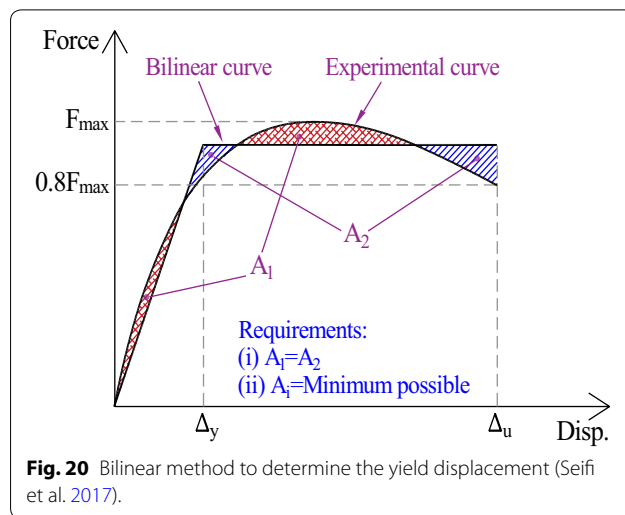
#### 4.2.3 Envelope Displacement Curves

The envelope of load–displacement curves of the specimens are shown in Fig. 19. Using this envelope curves, the peak load, ultimate displacement and ductility are calculated for normal concrete as well as for HPRCC specimens in negative and positive directions and presented in Table 8. To determine the yield displacement and to calculate the ductility, the method proposed by Paulay and Priestly (Paulay and Priestley 1992) is used and as it is shown in Fig. 20, idealized bilinear load–displacement response is obtained. To determine ultimate displacement ( $\delta_u$ ), the displacement corresponding to 20% reduction of peak load is considered (Paulay and Priestley 1992).

In contrast to the C2 specimen, the decreasing branch of the envelope curves for the other specimens are gradually reduced. As it is shown in Fig. 21, a comparison is made between the ratio of average peak load as well as the lower ductility factor of each specimen to those of C1 and C2 specimens. The average peak load of HPRCC specimens is increased by 3.12% and 21% compared to C1 and C2 specimen, respectively. Moreover, minimum ductility factor of SC2-A specimen increased by 6.8% and 24% compared to C1 and C2 specimens, respectively. Besides, the lower ductility factor of the SC2-B specimen reduced by 1.5% compared to that in C1 specimen and increased by 15% compared to that of C2 specimen.

#### 4.2.4 Energy Dissipation Capacity and Equivalent Hysteresis Damping Ratio

Energy dissipation capacity is the maximum dissipated energy by a structure that results in the slight or sudden collapse of the structure. According to Fig. 22, the area under a complete hysteretic loop at each cycle represents the energy dissipated by the specimen during that



cycle ( $E_i$ ) and the cumulative hysteresis energy dissipation capacity is calculated through summation of areas under the load–displacement hysteretic curve reversals ( $\sum E_i$ ) (Priestley and Macrae 1996; Shafaei et al. 2014). The most frequent and most obvious form of damping in structures is in the form of hysteresis of load–displacement response (Priestley and Macrae 1996; Shafaei et al. 2014). The equivalent damping ratio based on the parameters obtained from hysteresis behavior of beam–column connection specimens are calculated using Eq. 1. Hysteresis equivalent damping ratio ( $\xi_{eq}$ ) is the value of hysteresis energy dissipation of each cycle divided by energy dissipation of an equivalent normalized elastic cycle and is a good comparison criterion for quantifying the pinching effect (Priestley and Macrae 1996). According to Fig. 22,  $E_i$  is the energy dissipation in each cycle and is equal to the full area enclosed by load–displacement loop.  $A_e$  is representative of the stored elastic strain energy in an equivalent linear elastic system under static condition.

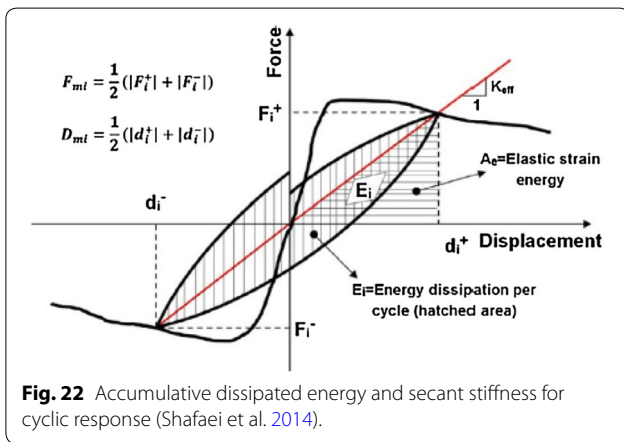
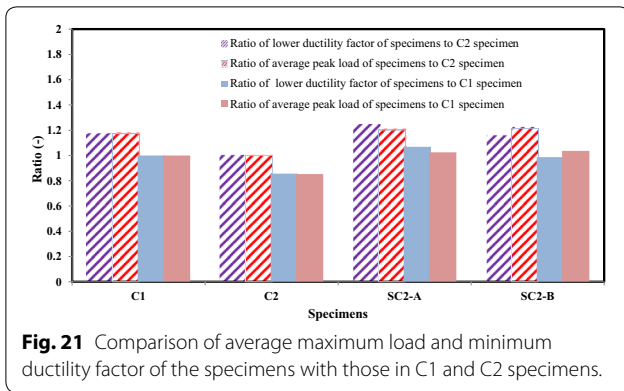
$$\xi_{eq} = \frac{1}{2\pi} \left( \frac{\text{area of loop}}{\text{area of triang}} \right) \tag{1}$$

$$\xi_{eq} = \frac{E_i}{2\pi P_{mi} D_{mi}} = \frac{E_i}{4\pi A_e} \tag{2}$$

$P_{mi}$  and  $D_{mi}$  in Eq. 2 represent the average peak load and displacement for the cycle  $i$ .

The cumulative energy dissipation and hysteresis equivalent damping ratio versus different drifts for each specimen are shown in Fig. 23.

As it can be seen in Fig. 23, in initial stages and before the drift of 2%, accumulative dissipated energy for normal concrete and HPRCC connection specimens is the same, since the elastic modulus of normal concrete and

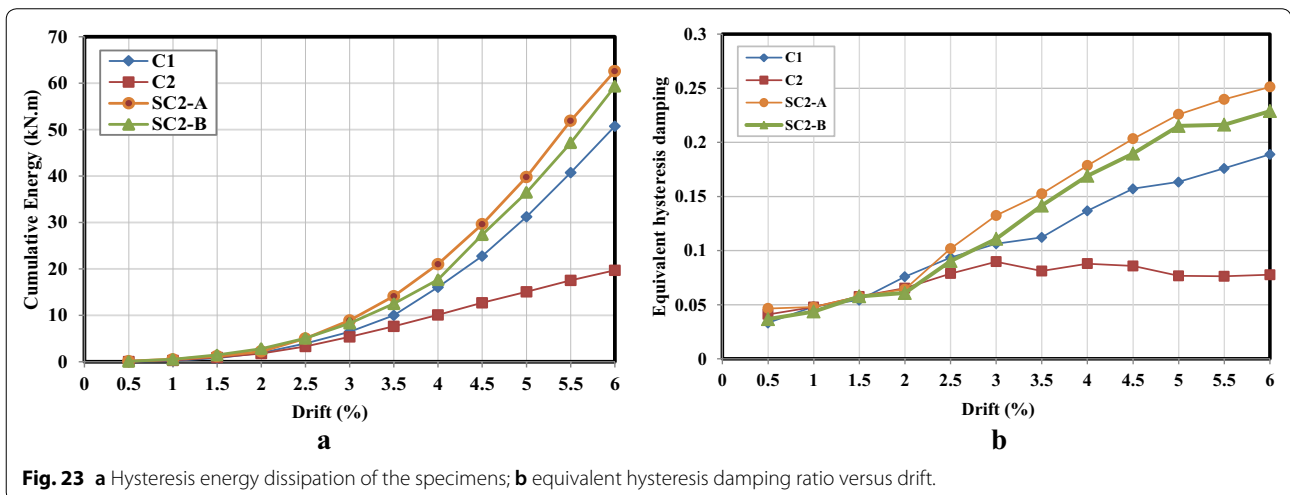


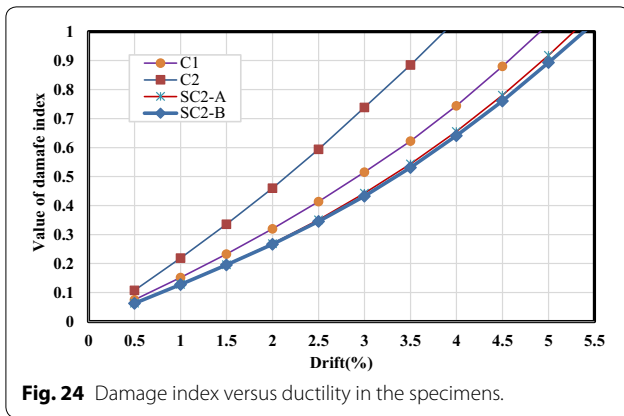
HPFRCC are close. After the drift of 2%, since the fibers cause bridging between cracks and prevent the propagation or opening of the cracks, the tensile strength, shear strength, ductility and energy dissipation capacity are improved and pinching effect in hysteresis loops

is minimized in HPFRCC beam-column connection. HPFRCC specimens have more energy dissipation capacity than normal concrete specimens do. The energy dissipated from the test beginning until the specimen drift of 6% for C1, C2, SC2-A and SC2-B specimens are 50.75, 19.74, 62.61 and 59.38 kN m respectively. As it can be seen, the average accumulative energy dissipation of HPFRCC specimens at drift of 6% is respectively 1.2 and 3.1 compared to that of C1 and C2 specimens. By increasing the drift after the yielding, SC2-A connection specimen has higher energy dissipation capacity compared to the other specimens, since HPFRCC-A material is more ductile (obtained by tension, compression and shear tests) compared to HPFRCC-B. For the drifts lower than 1.5%, equivalent hysteresis damping ratio of all specimens are approximately the same and is equal to 0.05, since the cracks are similar and damage is limited. By increasing the displacements, crack grow and concentration as well as yield of reinforcement cause the damping ratio to go up. But in C2 specimen after the drift of 3.5%, due to pinching and strength loss induced by shear fracture of joint, equivalent hysteresis damping ratio do not increase. In normal concrete specimen with seismic detailing and HPFRCC hysteresis loop area and damping ratio are increased due to the plastic hinge formation mechanism and absence of pinching. Equivalent damping factor ratio in normal concrete with seismic detailing reaches to 0.18 at drift level of 6%. This value for HPFRCC connection specimens is increased by 22% to 25% compared to that in C1 specimen.

**4.2.5 Damage Index**

As it can be seen in Fig. 24, Park et al. (1987) damage index is used for comparison of relative behavior of





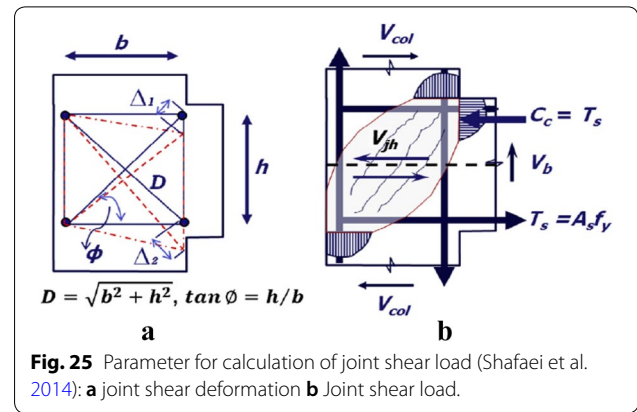
beam-column connections with/without HPCFRCC. Damage index is defined equation by 3.

$$DI = \frac{\delta_M}{\delta_u} + \frac{\beta}{F_y \delta_u} \int dE \quad (3)$$

where  $\delta_M$  is the maximum displacement demand under cyclic loading,  $\delta_u$  is the maximum displacement capacity under monotonic load, integral term is energy dissipation under cyclic load and  $F_y$  is structure yield strength and  $\beta$  is strength reduction factor that for a desirable concrete structure it is equal to 0.1 (Villemure 1995).

Values of  $\delta_M$ ,  $F_y$  and  $\int dE$  are obtained from the experimental results of the joint specimens, whereas the value of  $\delta_u$  that comprises contributions from deformations of beams, columns and joint, was estimated based on the empirical formula for the calculation of ultimate drift ratio according to CEN Eurocode 8 [43].

Damage index values [DI] vary from zero to 1, so that zero indicates no damage and 1 indicates a complete damage. In this study, it is assumed that in the case of DI in the range of  $0 < DI < 0.2$  represents elastic behavior or non-damage,  $0.2 < DI < 0.4$  represents a minor damage,  $0.4 < DI < 0.6$  represents moderate damage and  $0.6 < DI < 0.8$  represents serious damage and also in the case of  $DI > 0.8$  complete damage is occurred (Chidambaram and Agarwal 2015; Villemure 1995). HPCFRCC specimens always show lower damage at every drift than normal concrete specimens with/without seismic details during loading. C2 specimen suffers moderate damage, severe damage and complete collapse respectively at drift of 1.75, 2.5 and above 3.25%. C1 specimen suffers moderate damage, severe damage and complete collapse respectively at drift of 2.5, 3.5 and above 4.25%. Specimens SC2-A and SC2-B suffered moderate damage at drift between 2.75 and 3.75%, severe damage at drifts between 3.75 and 4.6%, and collapsed completely at drifts



higher than 4.6%. The measured drift at collapse stage in HPCFRCC specimens increases about 1.08 and 1.41 times as that of the normal concrete specimens with and without details. It is concluded that HPCFRCC specimens had a nearly 15% and 40% reduction in damage compared with normal concrete specimens with and without seismic details. This means that using HPCFRCC to improve the performance of the column-to-column connections is quite effective.

#### 4.2.6 Stress-Shear Deformation Response

As it can be seen in Fig. 25, the shear stresses ( $v_j$ ) and average shear deformation ( $\gamma_{ave}$ ) of connection are calculated using Eqs. (4, 7). It is assumed that HPCFRCC material has no participation in final bending strength of the beam. This assumption is correct for beams with reinforcement ratio greater than 1% under large rotations in the plastic hinge ( $\geq 0.03$  rad) because of significant fiber pull out. This situation is obviously observed in HPCFRCC connections. Moreover, the moment arm is assumed as  $jd = 0.9d$  for simplification since the internal tension load in beams is the result of tensile stresses in reinforcement and HPCFRCC material. The diagonal elongations  $\Delta_1$  and  $\Delta_2$  in the joint zone is measured by LVDT to calculate the shear deformation.  $D$  is the diameter of joint prior to deformation;  $\phi$  is the angle of the diagonal gauge with the horizonline, where  $\tan \phi = h/b$ ,  $h$  and  $b$  are respectively the vertical and horizontal distances between the end points of the diagonal gauge (see Fig. 25a) (Bedirhanoglu et al. 2013).

$$\gamma_{ave} = \frac{\Delta_1 + \Delta_2}{D \sin 2\phi} \quad (4)$$

$$V_{jh} = T_s - V_C \quad (5)$$

$$\tau_v = v_j = \frac{V_j}{A_j} \quad (6)$$

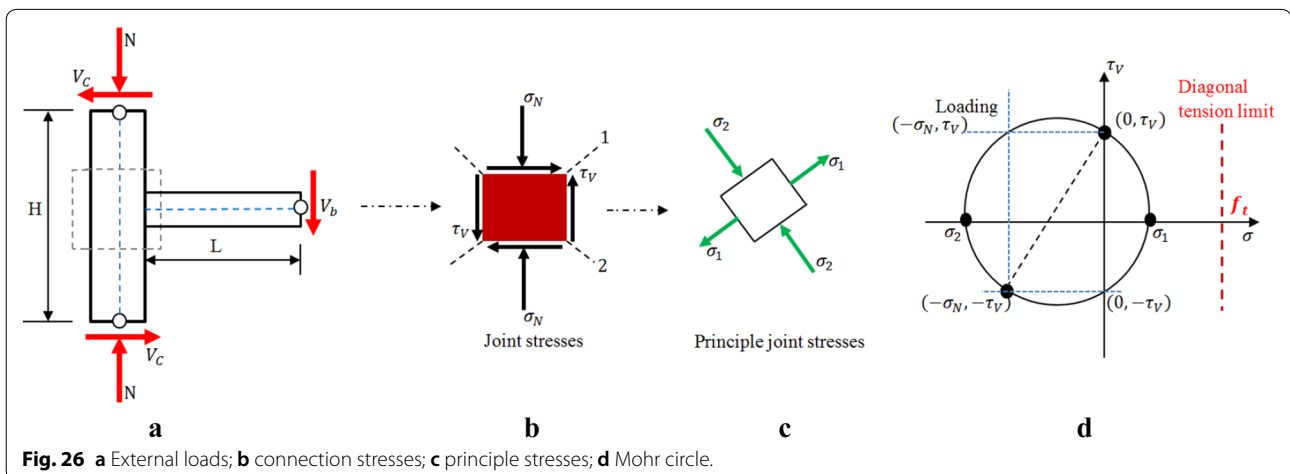
$$v_j = \frac{\sum \frac{M_{ub}}{jd} - V_C}{b_j h_c} \tag{7}$$

where  $T_s$  is tension load of beam longitudinal reinforcement,  $V_C$  is column shear,  $M_{ub}$  is ultimate bending strength of beams connected to column along the loading direction,  $JD$  is the distance between the resultant compression and tension internal loads in beams,  $b_j$  is the effective connection width and  $h_c$  is column width. Diagonal crack occurs when principle tension stress reaches the concrete tensile strength. Consequently, shear failure is a function of concrete tensile strength. It should be noted that principle stresses are calculated using Eq. 8 according to Mohr theory (Mohr 1900) using normal and shear stresses. When shear stress in a joint without confining reinforcement (transverse) induce tension stress higher than joint material tensile strength, cracking occurs in joint. The beam shear load ( $V_b$ ), column axial load ( $N$ ), and the induced shear and axial stresses and the related principle stresses in the joint core are shown in Fig. 26a–c. Mohr circle for these stresses is shown in Fig. 26d.

$$\sigma_{1,2} = \frac{\sigma_x + \sigma_y}{2} \pm \sqrt{\left(\frac{\sigma_x - \sigma_y}{2}\right)^2 + \tau_{xy}^2} \tag{8}$$

Connection specimens are designed in a way that the maximum shear in joint is close to the values recommended by ACI code (2011). This value is  $\sqrt{f'_c}$  MPa for exterior connections. In this shear stress level, it is possible to better evaluate the HSPFRCC material as a

replacement for transverse reinforcement in joint. It should be noted that the maximum shear stress in joint recommended by ACI code is for normal concrete structures and no design recommendation is provided for determination of connection allowable shear stress in beam-column HSPFRCC connection. The shear stress hysteretic behavior of the specimens versus shear deformation response is shown in Fig. 27. Table 9 summarizes the experimental results of each specimen. It shall be noted that recording shear deformations higher than drift of 4.5% was not possible due to crushing of C2 joint zone. As it is seen the behavior of the joint in HSPFRCC specimens is approximately linear with maximum shear stress required for joint equal to 5.49 MPa corresponding to  $0.81 \sqrt{f'_c}$  MPa that this level of shear stress causes tensile stress about 4.09 MPa corresponding to  $0.61 \sqrt{f'_c}$  MPa that is lower than average tensile strength 6.45 MPa for HSPFRCC materials obtained from the tension test (see Fig. 28a). While no observable crack is seen in the HSPFRCC joint zone and causes linear behavior and limited shear deformations in joint. In normal concrete specimen with seismic details, the maximum shear stress required for connection is equal to 5.83 MPa corresponding to  $1.03 \sqrt{f'_c}$  MPa that the tensile stress developed in normal concrete joint is higher than tensile strength 2.9 MPa while despite the existence of transverse reinforcing bars, cracking and damages are observed in the joint in this level of stress and causes shear deformations higher than HSPFRCC specimens. Also, in normal concrete specimen without seismic details, the maximum shear stress required for connection is equal to 4.38 MPa corresponding to  $0.77 \sqrt{f'_c}$  MPa that the tensile stress developed in normal concrete joint is higher than tensile strength 2.9 MPa (see Fig. 28a) while nonexistence of



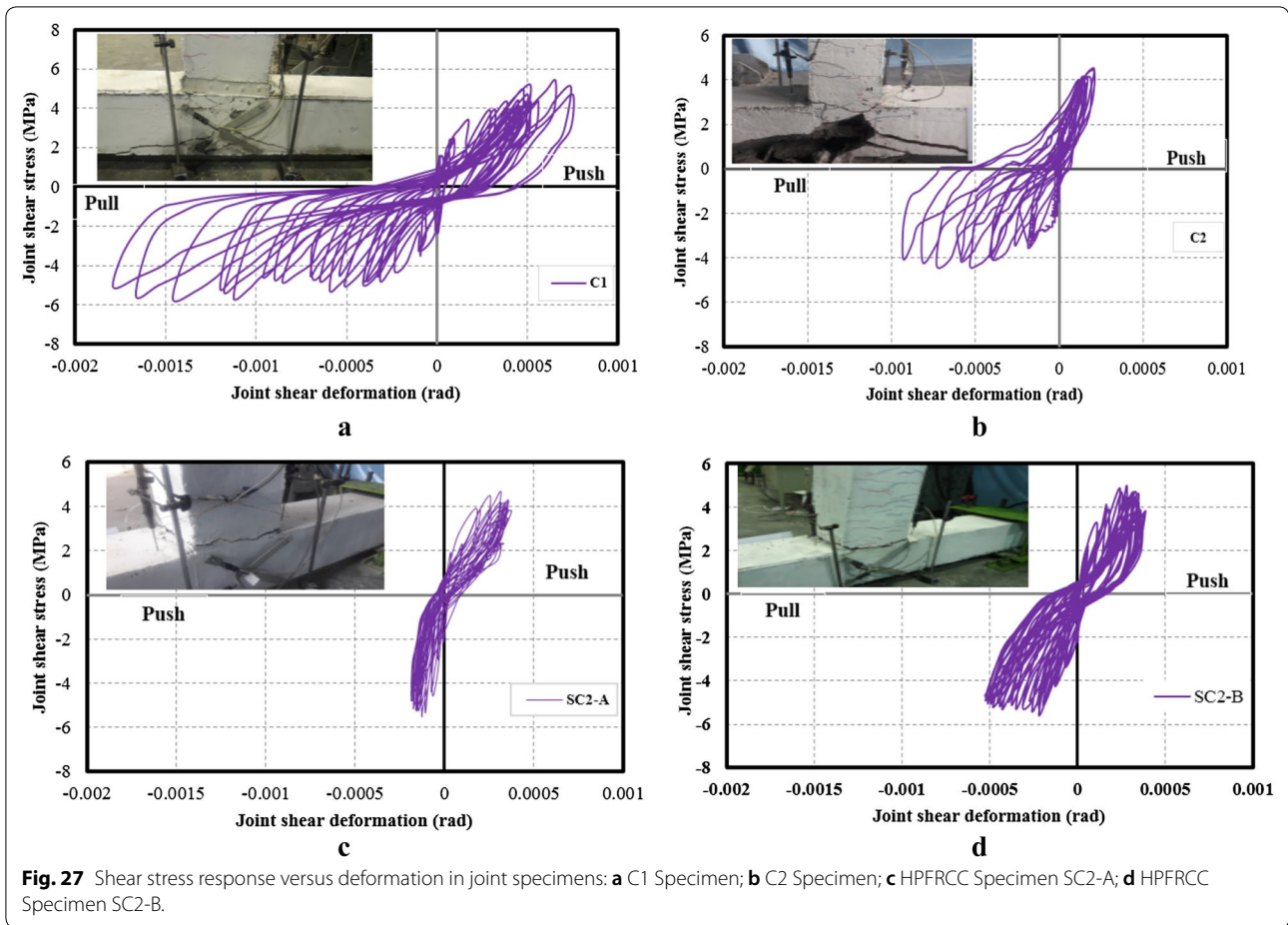


**Table 9** Summary of experimental results.

| Specimen | $\sigma_{pc}$ | $\epsilon_{pc}$ | $f'_c$ , MPa | $v_{jmax} / \sqrt{f'_c}$ | Failure mode     |
|----------|---------------|-----------------|--------------|--------------------------|------------------|
| C1       | 2.9           | 0.002           | 31.87        | 1.03                     | Flexural failure |
| C2       | 2.9           | 0.002           | 31.87        | 0.77                     | Shear failure    |
| SC2-A    | 6.2           | 0.07            | 41.47        | 0.86                     | Flexural failure |
| SC2-B    | 6.7           | 0.066           | 50.57        | 0.76                     | Flexural failure |

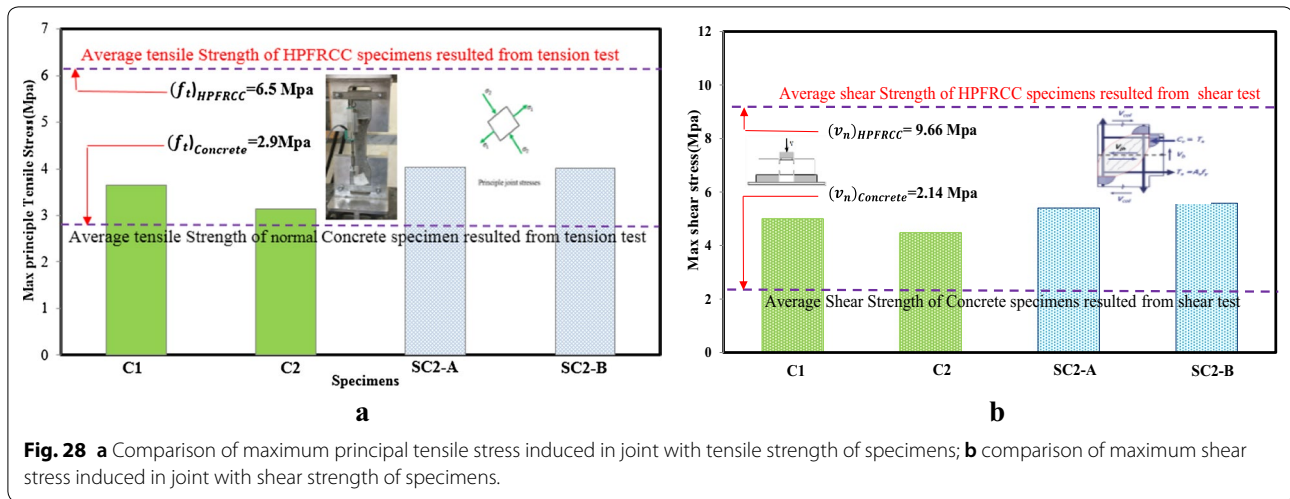
$\sigma_{pc}$  = post cracking (peak) tensile strength;  $\epsilon_{pc}$  = tensile strain capacity (strain at peak stress).

transverse reinforcing bars, cracking, high shear deformations and severe damages are observed in the joint in this level of stress that causes shear failure. In previous researches (Parra-Montesinos et al. 2005) the maximum shear stress in the internal beam-column connection without transverse reinforcement using HPCRCC is 9.3 MPa corresponding to  $1.4 \sqrt{f'_c}$  MPa and in reference research (Zhang et al. 2015), the maximum shear stress in the external beam-column connection without transverse reinforcement using ECC is obtained 2.2 MPa corresponding to  $0.35 \sqrt{f'_c}$  MPa.

The resulting shear and the related principle stresses in the joint core are compared with the shear and tensile strength of material, obtained by direct shear and uniaxial tension tests (see Fig. 28).

### 5 Conclusion

The results of this study are presented with the aim of providing a better understanding about the strain hardening behavior in high-performance fiber reinforced cement composites using uniaxial compression test, uniaxial tension test, and direct shear test. This material is used to fabricate beam-column connections with high strength against damage and to avoid the need for confining reinforcement (transverse) in joint. Two types of fiber cementitious materials are investigated in this paper including hooked steel and hybrid fibers (hooked steel fibers and macro synthetic fibers with 2% volume ratio). The four half scale specimens of exterior beam-column connections with seismic and without seismic reinforcement detail and identical dimensions are tested by applying lateral cyclic loading with increasing amplitudes. For the specimens without stirrups in the joint zone



(without seismic reinforcement detail), normal concrete is replaced with HSPFRCC in the joint zone. Based on the experimental observations and results, the following conclusions are drawn:

1. Results of tension and direct shear tests show that HSPFRCC specimens have strain hardening behavior accompanied by several cracks. Although no coarse aggregate is used in HSPFRCC specimens, the average elasticity modulus of cylindrical HSPFRCC specimens is close to that of normal concrete.
2. In all HSPFRCC beam-column connections, even in the case of the specimen without transverse reinforcement, adequate shear strength in the joint is provided by HSPFRCC material and no local shear crack is formed. This allows the formation of plastic hinges in beams and local damages in HSPFRCC material in the plastic hinge area.
3. The average peak load in HSPFRCC beam-column connection is higher than that of normal concrete with and without seismic details by 3.12% and 21% respectively. Moreover, the minimum ductility factor in HSPFRCC beam-column connections without seismic details using hybrid fiber and steel fiber is respectively 6.8% higher and 1.5% lower than that in normal concrete beam-column connection specimen with seismic details.
4. The ratio between average accumulative energy dissipation in HSPFRCC connections and in normal concrete connections with and without seismic details at the drift of 6% is respectively 1.2 and 3.1. Moreover the comparison of equivalent hysteresis damping ratio of connection at drift of 6% shows that the equivalent hysteresis damping of connections with hybrid fibers and with single steel fibers is respec-

tively 3.22 and 2.82 times as much as that of normal concrete connection without seismic details and 1.33 and 1.16 times as much as the equivalent hysteresis damping ratio of normal concrete connections with seismic details. This confirms the better behavior of hybrid fiber material than that of single steel fiber material from energy dissipation point of view.

5. HSPFRCC connections always show lower damage at any drift than that in normal concrete connections with/without seismic details during the loading process. The drift at collapse step in HSPFRCC connections has increased by about 1.08 and 1.41 times as that in the normal concrete connections with and without details. It is concluded that HSPFRCC specimens had a nearly 15% and 40% reduction in damage compared with normal concrete specimens with and without seismic details. This means that the use of HSPFRCC to improve the performance of the column-to-column connections is quite effective.
6. Design of beam-column connection is conducted in a way that the shear stresses induced in joint are close to the values recommended by ACI code, i.e.  $\sqrt{f'_c}$  MPa. The behavior of the connection in HSPFRCC specimens is approximately linear. While in normal concrete connection with seismic details, the great inelastic deformations and damages can occur in joint under shear loads close to the shear strength of the connection. On the other hand, the HSPFRCC connections show approximately linear elastic response with partial damages in connection with this level of shear stress. Moreover, the shear stress limit in accordance with ACI standard codes for lateral connections to be applied in HSPFRCC connections without confinement (transverse) reinforcement is sufficient.

**Authors' contributions**

MH-S: the main researcher, design and conduction of the tests, initial writing of the paper, data analyzer. H-S: researcher of the seismic tests, supervisor of the tests, supervisor of data analyses, paper editor. AK: material part research, supervisor of the tests, supervisor of data analyses, paper editor. All authors read and approved the final manuscript.

**Author details**

<sup>1</sup> Department of Civil Engineering, Ferdowsi University of Mashhad, P.O. Box 91775-1111, Mashhad, Iran. <sup>2</sup> Department of Civil Engineering, Semnan University, Semnan, Iran.

**Acknowledgements**

Not applicable.

**Competing interests**

Authors declare that they have no competing interests.

**Availability of data and material**

Not applicable.

**Funding**

Not applicable.

**Publisher's Note**

Springer Nature remains neutral with regard to jurisdictional claims in published maps and institutional affiliations.

Received: 6 October 2017 Accepted: 19 October 2018

Published online: 30 January 2019

**References**

- A.C. Building Code Requirements for Structural Concrete (ACI 318-11M) and Commentary. (2011). American Concrete Institute.
- ASTM, & C39/C39M-10. (2010). *Standard test method for compressive strength of cylindrical concrete specimens* (p. 7). West Conshohocken: American Society of Testing and Materials.
- Bayasi, Z., & Gebman, M. (2002). Reduction of lateral reinforcement in seismic beam-column connection via application of steel fibers. *Structural Journal*, 99(6), 772–780.
- Bedirhanoglu, I., Ilki, A., & Kumbasar, N. (2013). Precast fiber reinforced cementitious composites for seismic retrofit of deficient RC joints—a pilot study. *Engineering Structures*, 52, 192–206.
- Bindhu, K., & Jaya, K. (2010). Strength and behaviour of exterior beam column joints with diagonal cross bracing bars. *Asian Journal of Civil Engineering (Building and Housing)*, 11(3), 397–410.
- Chidambaram, R. S., & Agarwal, P. (2015). Seismic behavior of hybrid fiber reinforced cementitious composite beam-column joints. *Materials and Design*, 86, 771–781.
- Craig, R. J., et al. (1984). Behavior of joints using reinforced fibrous concrete. *Special Publication*, 81, 125–168.
- Durrani, A. J. & Wight, J. K. (1982). Experimental and analytical study of internal beam to column connections subjected to reversed cyclic loading.
- Ehsani, M. R. & Wight, J. K. (1982). Behavior of external reinforced concrete beam to column connections subjected to earthquake type loading.
- Elwood, K. J., et al. (2007). Update to ASCE/SEI 41 concrete provisions. *Earthquake Spectra*, 23(3), 493–523.
- Filiatrault, A., Pineau, S., & Houde, J. (1995). Seismic behavior of steel-fiber reinforced concrete interior beam-column joints. *ACI Structural Journal*, 92(5), 543–552.
- Gefken, P. R., & Ramey, M. R. (1989). Increased joint hoop spacing in type 2 seismic joints using fiber reinforced concrete. *ACI Structural Journal*, 86(2), 168–172.
- Hemmati, A., Kheyroddin, A., & Sharbatdar, M. K. (2013). Plastic hinge rotation capacity of reinforced HPFRCC beams. *Journal of Structural Engineering*, 141(2), 04014111.
- Hemmati, A., et al. (2016). Ductile behavior of high performance fiber reinforced cementitious composite (HPFRCC) frames. *Construction and Building Materials*, 115, 681–689.
- Henager, C. (1977). Steel Fibrous-Ductile concrete joint for seismic-resistant structures. *Special Publication*, 53, 371–386.
- Hossein Saghafi, M., & Shariatmadar, H. (2018). Enhancement of seismic performance of beam-column joint connections using high performance fiber reinforced cementitious composites. *Construction and Building Materials*, 180, 665–680.
- Jiuru, T., et al. (1992). Seismic behavior and shear strength of framed joint using steel-fiber reinforced concrete. *Journal of Structural Engineering*, 118(2), 341–358.
- JSCE. (2008). Recommendations for design and construction of high performance fiber reinforced cement composites with multiple fine cracks (HPFRCC). In *Concrete engineering series no. 82*.
- JSCE, G 553-1999. (2005). Test method for shear strength of steel fiber reinforced concrete. Standard Specifications for Concrete Structures. In *Test methods and specifications* (pp. 362).
- Kim, D. J., Naaman, A. E., & El-Tawil, S. (2008). Comparative flexural behavior of four fiber reinforced cementitious composites. *Cement & Concrete Composites*, 30(10), 917–928.
- Megget, L., & Park, R. (1971). Reinforced concrete exterior beam-column joints under seismic loading. *New Zealand Engineering*, 26(11), 341.
- Metelli, G., et al. (2015). A model for beam-column corner joints of existing RC frame subjected to cyclic loading. *Engineering Structures*, 89, 79–92.
- Mirsayah, A. A., & Banthia, N. (2002). Shear strength of steel fiber-reinforced concrete. *Materials Journal*, 99(5), 473–479.
- Mohr, O. (1900). Welche Umstände bedingen die Elastizitätsgrenze und den Bruch eines Materials. *Zeitschrift des Vereins Deutscher Ingenieure*, 46(1524–1530), 1572–1577.
- Naaman, A. (1996). Characterization of high performance fiber reinforced cement composites-HPFRCC. *High Performance Fiber Cement Composites (HPFRCC2)*, 2, 1–23.
- Park, Y., Ang, A. H., & Wen, Y. (1987). Damage-limiting aseismic design of buildings. *Earthquake Spectra*, 3(1), 1–26.
- Parra-Montesinos, G. J., Peterfreund, S. W., & Chao, S.-H. (2005). Highly damage-tolerant beam-column joints through use of high-performance fiber-reinforced cement composites. *ACI Structural Journal*, 102(3), 487.
- Paulay, T. & Priestley, M. N. (1992). Seismic design of reinforced concrete and masonry buildings.
- Priestley, M. N., & Macrae, G. (1996). Seismic tests of precast beam-to-column joint subassemblies with unbonded tendons. *PCI Journal*, 41(1), 64–81.
- Qudah, S., & Maalej, M. (2014). Application of engineered cementitious composites (ECC) in interior beam-column connections for enhanced seismic resistance. *Engineering Structures*, 69, 235–245.
- Saghafi, M., Shariatmadar, H., & Kheyroddin, A. (2016). Experimental study and application of high performance fiber reinforced cementitious composites for retrofitting beam-column joints in rigid-framed railway bridges.
- Saghafi, M. H., Shariatmadar, H., & Kheyroddin, A. (2017). Experimental evaluation of mechanical properties of high performance fiber reinforced cementitious composites. *Concrete Research (JCRE)*, 9(2), 29–42.
- Said, S. H., & Razak, H. A. (2016). Structural behavior of RC engineered cementitious composite (ECC) exterior beam-column joints under reversed cyclic loading. *Construction and Building Materials*, 107, 226–234.
- Seifi, A., et al. (2017). Improving seismic performance of old-type RC frames using NSM technique and FRP jackets. *Engineering Structures*, 147, 705–723.
- Shafaei, J., Hosseini, A., & Marefat, M. S. (2014a). Seismic retrofit of external RC beam-column joints by joint enlargement using prestressed steel angles. *Engineering Structures*, 81, 265–288.
- Shafaei, J., et al. (2014b). Effects of joint flexibility on lateral response of reinforced concrete frames. *Engineering Structures*, 81, 412–431.
- Villemure, I. (1995). Damage indices for reinforced concrete frames: evaluation and correlation. University of British Columbia.
- Yuan, F., et al. (2013). A comparison of engineered cementitious composites versus normal concrete in beam-column joints under reversed cyclic loading. *Materials and Structures*, 46(1–2), 145–159.
- Zhang, R., et al. (2015). Application of PP-ECC in beam-column joint connections of rigid-framed railway bridges to reduce transverse reinforcements. *Engineering Structures*, 86, 146–156.